TECHNICAL MEMORANDUM

481

Ice supersaturation in the ECMWF Integrated Forecast System

A. M. Tompkins[1], K. Gierens[2], G. Rädel[3]

Research Department

[1]ECMWF, UK [2] DLR, Germany [3] University of Reading, UK

December 14, 2005

European Centre for Medium-Range Weather Forecasts
Europäisches Zentrum für mittelfristige Wettervorhersage
Centre européen pour les prévisions météorologiques à moyen terme

Series: ECMWF Technical Memoranda

A full list of ECMWF Publications can be found on our web site under:
http://www.ecmwf.int/publications/

Contact: library@ecmwf.int

European Centre for Medium-Range Weather Forecasts
Shinfield Park, Reading, RG2 9AX, England

Abstract

A simple parameterisation for ice supersaturation is introduced into the ECMWF IFS model, compatible with the cloud scheme that allows partial cloud coverage. It is argued that many existing schemes that explicitly represent the ice nucleation process without prognosing the humidity evolution separately in the clear sky and cloudy portions of a model grid-cell are subject to artificial subgrid-scale horizontal water vapour transfer, possibly dominating the scheme's behaviour. Here this is avoided by making the simple but justifiable diagnostic assumption that the nucleation process is fast compared to a GCM timestep, thus supersaturation is only permitted in the clear-sky portion of the gridcell.

Results from model integrations using the new scheme are presented. It is shown that the new schemes increases upper-tropospheric humidity, decreases high level cloud cover and to a much lesser extent cloud ice amounts, all as expected from simple arguments. The increases in humidity are expected to be beneficial, since much evidence points to a model dry bias in the upper troposphere. The relative distribution of supersaturation occurrence is found to reproduce the observed climatology derived from in situ aircraft observations very well. It is also demonstrated that the new scheme leads to improved predictions of permanent contrail cloud over Southern England, which indirectly implies upper-tropospheric humidity fields are better represented for this region.

1 Introduction

While clouds are commonly cited as an important but ill-understood component of atmospheric models of all spatial and temporal scales, it is ice cloud processes that are the least understood. It is only very recently that initial attempts have been possible to supplement in-situ (and thus extremely sparse) aircraft data (e.g. Heymsfield et al., 1998) with global remotely sensed observations of basic ice cloud information such as the ice water content or crystal habits (e.g. Rädel et al., 2003; Li et al., 2005).

One of the complexities of ice clouds is that unlike liquid water clouds, the ice nucleation process in the atmosphere can occur via both homogeneous and heterogeneous pathways (Pruppacher and Klett, 1997), with the latter further subdivided into a number of nucleation mechanisms. This work only considers the former homogeneous process, which is supposed to dominate cirrus cloud formation in the presence of moderate or stronger up-draughts, or in relatively pristine environments with few ice condensation nuclei present (Spice et al., 1999; Lin et al., 2002; Gierens, 2003; Ren and Mackenzie, 2005). The lack of consideration of plethora of heterogeneous processes is noted as a caveat in this work.

Ice crystal nucleation contrasts sharply with the equivalent process for liquid cloud droplets, since the nucleation process is not activated at small supersaturations with respect to the ice saturation vapour pressure. At cold temperatures, where the difference between the liquid water and ice saturation vapour pressures is large, the relative humidity (RH) with respect to ice can exceed 150% before the onset of the nucleation process, and supersaturations with respect to ice are commonly observed by in-situ and remote sensing techniques (e.g. Heymsfield et al., 1998; Gierens et al., 1999, 2000, 2004; Spichtinger et al., 2003). This is illustrated schematically in panel *a* of Fig. 1 which shows the hypothetical evolution of a upper troposphere parcel of air subjected to adiabatic cooling. Panel *a* illustrates that RH increases until a critical threshold is reached (RH_{crit}) that can significantly exceed the 100% saturated value which marks the onset of condensation in liquid water clouds. At this critical value ice crystals are homogeneously nucleated and their uptake of the excess water vapour prevents the RH from rising much past RH_{crit}, and in fact the RH then reduces towards a value that in most cases just exceeds the 100% level. The depositional growth timescale may be shorter or longer than a GCM timestep, but is however generally short compared to the time required to reach the critical value needed to initiate nucleation. It is clear that the zero order effect of modelling the ice nucleation process explicitly is that significant supersaturation in a GCM grid-cell is possible.

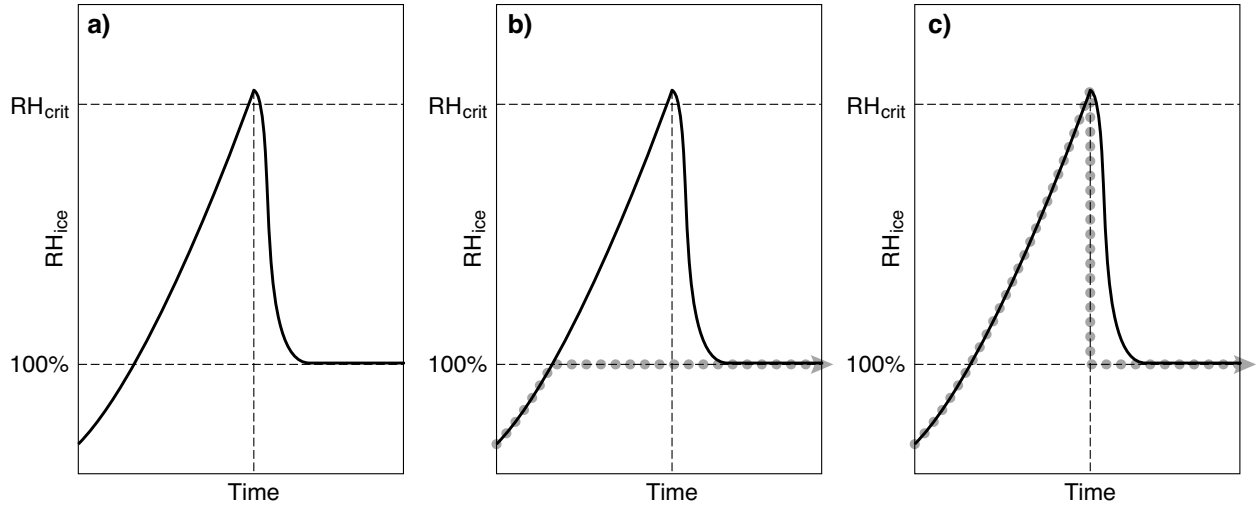

Figure 1: Schematic (adapted from Lohmann and Kärcher (2002) of the evolution of relative humidity (RH) in a hypothetical parcel subject to adiabatic cooling at cold temperatures (T<232K). In panel (b) a dotted line is added to indicate the approximation of this process by the operational ECMWF IFS code. The present scheme does not allow RH to exceed 100%, and any excess humidity is instantaneously converted to ice. Panel (c) on the right outlines the new simple parametrization described in this paper. The new scheme allows supersaturation to occur and thus represents the hysteresis in the ice cloud behaviour. However, the scheme does not attempt to explicitly model the nucleation process itself and converts all humidity exceeding the saturation value to ice instantaneously once the nucleation threshold is attained. It should be emphasised that the scheme attempts to ascertain how much of the grid box has reached this threshold and the adjustment only occurs inside this cloudy region of the gridbox. Thus grid-mean supersaturated states can be maintained even in gridboxes that contain some ice.

Many models currently treat the ice phase similarly to warm-phase microphysical processes, in that supersaturation is immediately converted to ice crystals. The ECMWF integrated forecast system (IFS) is one such model (shown in panel *b* of Fig.1). It is to be expected that such models will suffer from upper troposphere dry biases and underestimate humidity temporal and spatial variability and Ovarlez and van Velthoven (1997); Ovarlez et al. (2000) show this to be the case for earlier versions of the IFS. In order to rectify this shortcoming in the IFS ice microphysics, this document outlines a simple parametrization which modifies a saturation-adjustment-type scheme in the ECMWF IFS in order to take the nucleation process into account consistently with the assumptions concerning the grid cloud cover.

2 Homogeneous nucleation in large-scale models

Relative to heterogeneous ice nucleation, the homogeneous nucleation process is reasonably well understood. Classical theory and controlled laboratory experiments have documented the critical vapour saturation mixing ratio with respect to ice at which homogeneous ice nucleation initiates (Pruppacher and Klett, 1997; Koop et al., 2000). This work adopts the supersaturated relative humidity threshold RH_{crit}[1] using the empirical approximation of the results of Koop et al. (2000) given by Kärcher and Lohmann (2002), which is a function of temperature and ranges from 45% supersaturation at $T = 235$ K to 67% at $T = 190$ K.

This threshold is a local condition, describing nucleation in a well mixed parcel of air of unspecified dimen-

[1]Since the IFS only has one cloud water variable, *RH* is calculated with respect to liquid water in the warm phase (T >273K) and with respect to ice when temperatures are colder than 250K. Between these values it is interpolated according to Simmons et al. (1999). However, since this work considers pure ice phase clouds only, *RH* refers to the ice saturated value throughout.

Scheme	environment humidity q_v^e	in-cloud humidity q_v^c
ECHAM4 (Lohmann and Kärcher, 2002)	q_v	q_v
Gierens (personal communication)	q_v+q_i	$q_v - q_i \frac{1-C}{C}$
Met Office UM (PC2) (Wilson and Forbes, 2004)	$CRH_{crit} q_s + (1-C)q$	$\frac{q-(1-C)q_v^e}{C}$
New parametrisation	$\frac{q_v - Cq_s}{1-C}$	q_s

Table 1: Diagnostic assumptions used by various existing schemes that aim to represent ice supersaturated states. Here q_v, q_i and q_s represent the grid-mean vapour, ice and saturation (with respect to ice) mixing ratios, respectively. A pure ice phase cloud is presumed, thus liquid water is neglected.

sions. It is unlikely to apply to a General Circulation model (GCM) with grid cell sizes spanning O(100km) in the horizontal and of finite vertical dimension. This is because over such a spatial scale, water vapour and temperature are likely to vary considerably. Thus the critical threshold for ice formation may be exceeded locally within the grid scale, while the grid mean values imply clear-sky conditions predominate. To accurately model the ice nucleation process therefore, knowledge of subgrid fluctuations are required.

A number of so-called statistical schemes are able to provide such information explicitly (e.g. Smith, 1990; Bony and Emanuel, 2001; Tompkins, 2002). However, most GCMs that do not have explicit representation of subgrid variability are still able to provide some information, the most basic of which is the provision of a fractional cloud cover, which determines exactly what portion of the grid cell contains cloud condensates and thus is subject to microphysical processes.

The fact that microphysics processes are only operating in the cloudy portion of the grid box presents a dilemma if one wishes to represent ice nucleation processes accurately. Outside the cloudy area highly supersaturated states may be maintained, while deposition can rapidly (i.e. fast compared to a typical GCM model timestep) deplete available supersaturation within the cloudy region. To model this accurately in a GCM from time-step to time-step a memory of the humidity both inside and outside the cloudy region is necessary. With only one prognostic equation usually used in GCMs for the grid-mean humidity, this means that either an additional prognostic equation is required (the environmental humidity for example) or simplifying diagnostic assumptions (a diagnostic parametrisation) need to be applied to divide the grid mean humidity between the cloudy and clear sky portions.

Previous schemes have used a variety of approaches to do this, outlined in table 1. All of these approaches suffer from a common drawback, which is illustrated with the example of the Lohmann and Kärcher (2002) scheme, which makes the simplest assumption that the environmental humidity equals the grid averaged value. We imagine a grid box that is half covered by cloud at a certain point in time and for which the humidity everywhere inside the grid-cell (both inside and outside the cloud) is exactly equal to the grid mean value, which is assumed ice supersaturated. Inside the cloud, ice crystals will grow at the expense of the supersaturation, and humidity will be depleted. Thus at the subsequent time-step the environmental humidity should exceed the in-cloud value, neglecting all other processes. However, since the scheme lacks a memory for this process,

one must resort to the diagnostic assumption of equal humidity in the clear-sky and cloudy portions. This equates to an artificial horizontal flux of humidity from the clear-sky to the cloudy portion of the domain. When each of the existing schemes in table 1 are considered in the context of microphysical processes, it is apparent that each features such a subgrid horizontal water vapour flux. It should be emphasised that this is not an inconsequential aspect of these schemes. The performance of the unified model is found to be critically sensitive to this assumption concerning humidity (D. Wilson, personal communication). Note also that the environmental and cloudy region humidities in the unified model parametrisation do not sum to give the grid mean value.

3 New scheme for the IFS

A very simple (i.e. with no new prognostic equations) scheme is presented which is tested in the ECMWF integrated forecast system (IFS) model. It attempts to represent the ice supersaturation and the homogeneous nucleation process in the IFS while excluding artificial horizontal water vapour transport on the subgrid-scale.

The scheme assumes the following:

(i) Ice nucleation initiates when the supersaturation *locally* reaches the threshold specified by Kärcher and Lohmann (2002).

(ii) As in the Tiedtke (1993) scheme, the clear-sky humidity fluctuations are assumed to be uniformly distributed with a fixed constant variance. Thus nucleation can occur when the grid-mean RH exceeds a threshold that is lower than the local criterion.

(iii) Once ice is present, the deposition process is sufficiently rapid relative to a GCM time-step that it can be approximated by a diagnostic adjustment to exactly saturated conditions inside the cloud.

A schematic summary of assumptions (i) and (iii) on which the new scheme is based is shown in panel c of Fig. 1. This schematic portrays the evolution of a homogenous air parcel, and thus does not represent point (ii) which concerns the subgrid-variability issue.

The main difference from existing schemes is the choice of assumption (iii), which appears to be reasonably justified in a wide range of updraught situations by modelling of the homogeneous nucleation process (Khvorostyanov and Sassen, 1998). The advantage of the above set of assumptions is that no artificial flux of humidity is permitted between clear-sky and cloudy regions. The obvious drawback is that clouds may not exist in subsaturated conditions, and no information concerning the ice crystal number concentration is available.

Given the parametrization assumption outlined in (iii), the assumption that the in-cloud humidity is equal to the saturation value q_s, allows one to derive the clear-sky humidity, q_v^e, given in table 1. This derivation for q_v^e is familiar since it is already assumed by the operational Tiedtke scheme (Jakob, 2000). However, the subtle difference in the new scheme is that the grid-mean humidity is now allowed to exceed the saturated value in the pure-ice phase. This means that previously q_v^e was constrained to be less than the saturated value, while the new scheme allows the humidity in the clear-sky to exceed that in the cloudy portion of the domain (as indeed it must do if the grid-mean is saturated). With this assumption therefore, the clear-sky 'memory' of humidity is retained through the separate prognostic evolution of the cloud cover.

If a cooling or other thermodynamic process increases the clear-sky humidity beyond the nucleation threshold specified by Kärcher and Lohmann (2002), the cloud cover, C, is appropriately increased. Practically, the scheme calculates the increase in cloud cover resulting from a temperature decrease ΔT as in the Tiedtke

(1993) scheme [2] as

$$\Delta C = -(1-C)\frac{\frac{dq_s}{dT}\Delta T}{2(RH_{crit}q_s - q_v^e)}, \quad (1)$$

with the associated change in ice mass mixing ratio given as

$$\Delta q_i = -0.5\Delta C\frac{dq_s}{dT}\Delta T. \quad (2)$$

This term only operates when the $q_v^e > K.RH_{crit}q_s$, (where the constant K is set to 0.8 throughout most of the troposphere), in other words when the relative humidity (RH) exceeds 80% of the threshold for nucleation. The value of 80% is a fixed diagnostic assessment of the horizontal temperature and humidity variability of the atmosphere. In the temperature range in which all cloud is assumed pure ice cloud in the IFS (T <250K), the RH_{crit} is set to the minimum of the critical supersaturated threshold given by Kärcher and Lohmann (2002) and the saturation mixing ratio with respect to liquid water. For warmer temperatures RH_{crit}=1, and the cloud source term reverts to the default scheme.

This change in ice mass will leave the q_v^c in a supersaturated state, which is then corrected by clipping the grid-mean humidity to the limit of

$$q_v^{max} = q_s(C + (1-C)RH_{crit}). \quad (3)$$

This clipping term has the effect of reducing the in-cloud humidity to the saturated value within one time-step. Again, with RH_{crit} equal to unity when T >250K a standard clipping to the saturation value is used.

4 Results

4.1 Model climate impact

Two 13-month T95 model integrations are conducted to investigate the effect of the modified cloud scheme. The control integration uses the default cloud scheme of model cycle 28r3. In terms of the model cloud climatology, the largest sensitivity was not in the total column ice water (TCIW, sometimes referred to as the ice water path) but rather the total cloud cover. Fig. 2 shows that the high cloud cover is reduced by the new scheme, as expected, since humidity must now attain higher values to initiate cloud formation. Compared to the relative reduction in high cloud cover of 17%, the global reduction in TCIW is much more modest at only 3%. Using ISCCP D2 retrievals of total cloud cover (Rossow and Schiffer, 1991, 1999) as a benchmark, the standard model previously tended to slightly but consistently overestimate the cloud cover throughout the deep convective areas in the tropics, especially over the Pacific and Indian Oceans, and also the over the south American continent (Tompkins et al., 2004; Jung et al., 2005). With the reduction in cloud cover associated with the new scheme, the biases are improved throughout the tropics with the exception of the Western Pacific warm pool, where the new scheme overcompensates and leads to an under-prediction of cloud cover (not shown).

The lower sensitivity of the ice water can be understood in terms of the relationship of the two metrics to the total water relative humidity ($RH_t = (q_v + q_i)/q_s$). In the default model where supersaturation is not allowed, the cloud cover is constrained to be 100% by definition as soon as RH_t exceeds unity, while with the new parameterisation much higher values of RH_t must be achieved for an overcast grid box. Cirrus clouds will therefore occur more rarely in the new scheme. However the sensitivity of the ice water path will be lower since once the higher threshold is reached in the new scheme, all of the water vapour exceeding the saturation mixing ratio is rapidly converted to ice, thus the ice content of these clouds is ultimately the same.

[2] Note that an error in the original scheme in this term was corrected by Jakob (2000)

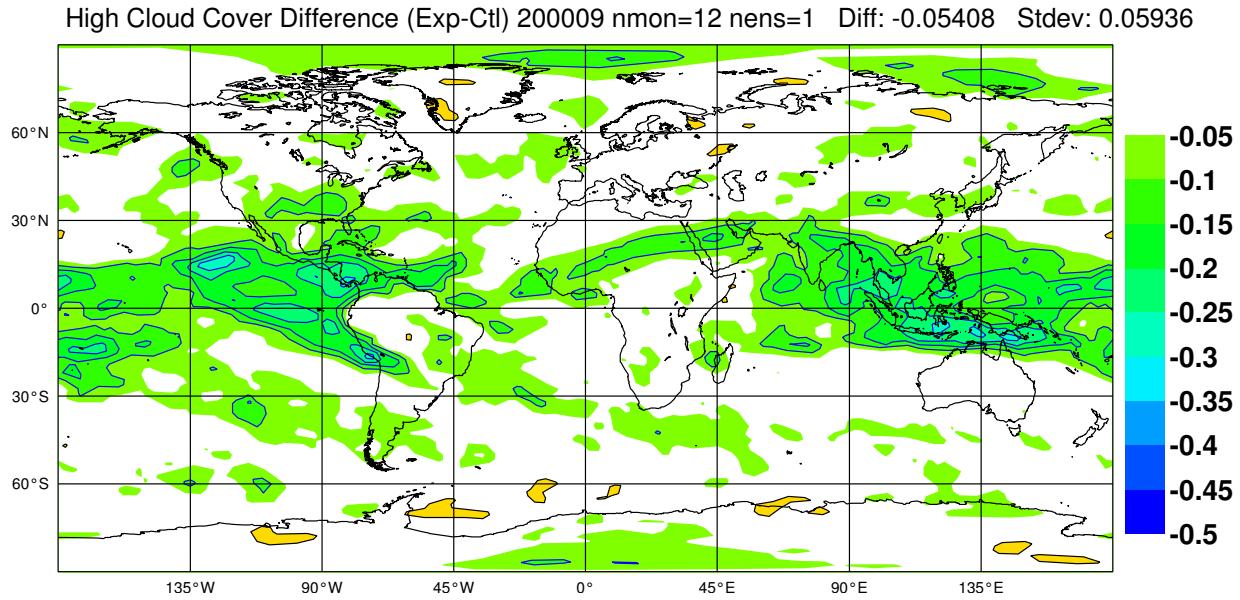

Figure 2: 12 month average difference in high cloud cover (p<450 hPa approximately) between two experiments using the new nucleation parametrisation and the control, respectively.

This can be illustrated with a straightforward scenario of two adjacent gridboxes in the upper atmosphere, with a temperature such that the critical RH for homogeneous nucleation is 140%. Starting from dry conditions, vertical motion causes one gridbox to attain $RH_t = 1.05$ and in the second, $RH_t = 1.45$. With the default model, both gridboxes become overcast, while with the new parametrization only the second gridbox becomes overcast. Therefore the cloud cover is 50% less with the new scheme. However, the evolution of the ice mass will be starkly different to the cloud cover. While the total water only just exceeds the modified threshold of $RH = 140\%$ in the second gridbox, once this threshold is exceeded the nucleation process immediately converts all the water vapour exceeding the saturation mixing ratio to ice, thus the final ice mass is identical with the default model and the new scheme. Therefore it is clear that the total ice mass averaged over the two gridboxes only reduces by 10% with the new scheme in this simple hypothetical example, much less than the 50% cloud cover reduction[3].

The impact of the supersaturation scheme on the humidity field is shown as a zonal mean difference in RH in Fig. 3. As expected the scheme increases relative humidity significantly in the upper troposphere and lower stratosphere quite significantly. The absolute increases in zonal mean RH are mostly in the range of 5 to 10%, with the peaks occurring in the troposphere/stratosphere transition zone above the main deep convective detrainment level in the tropics, and in the lower stratosphere at high latitudes. The peak in the tropics between the radiative and temperature tropopauses is expected since in this zone the atmosphere is subjected to gentle ascent, the diabatic cooling of which balances the small radiative heating. Further comments on the impact on the humidity field are given below.

[3]The cycle 28r3 ice microphysics will act to further homogenise the ice fields between the two case, since ice sedimentation is used as a proxy for the conversion of ice to snow (see Jakob, 2000, for more details). However even the application of more usual approaches to representation of the nonlinear process of snow generation (e.g. Lin et al., 1983) will not alter this above interpretation significantly since eventual ice amounts in the second gridbox are almost identical; only the temporal evolution differs.

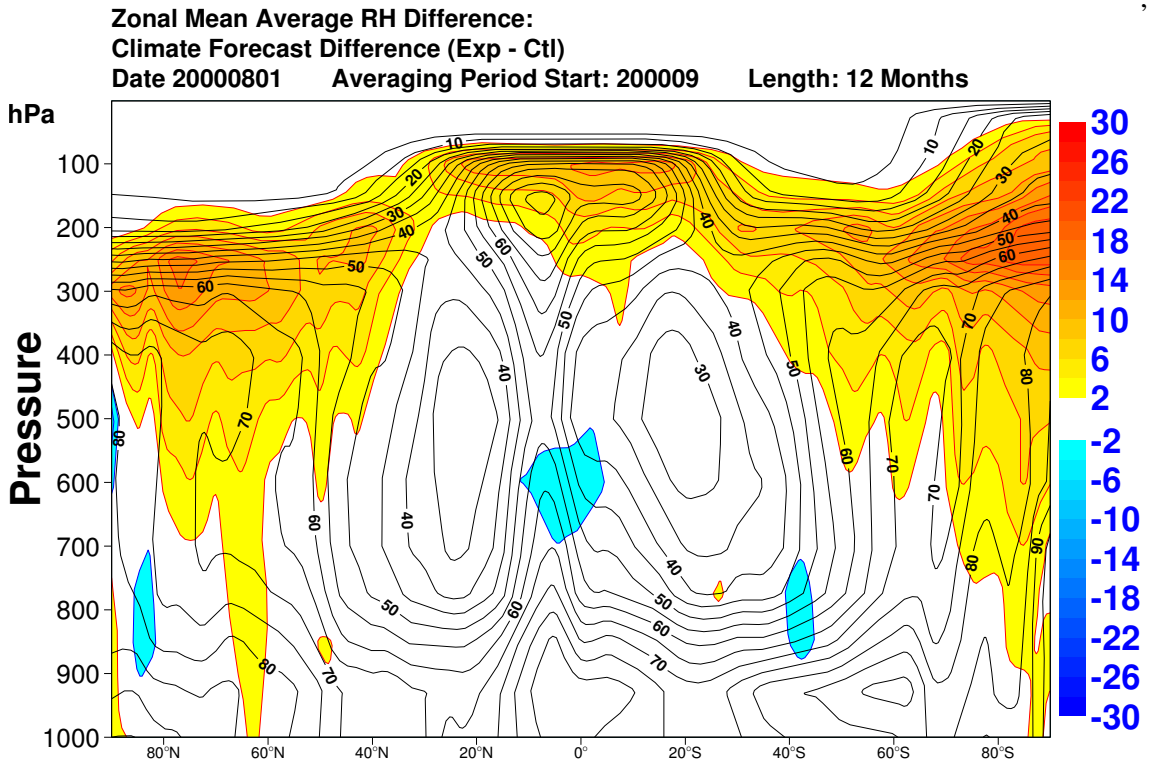

Figure 3: The shaded contours 12 month zonal mean average difference in relative humidity between two experiments using the new nucleation parametrisation and the control, respectively. The line contours give the relative humidity in the control forecast (contour interval is 5%).

4.2 Comparison to MOZAIC aircraft data

The humidity fields in the two year-long integrations described above are compared to aircraft data from the MOZAIC campaign, which compiled many years of in situ aircraft measurements taken by commercial aircraft carrying research quality instrumentation (Gierens et al., 1999). A third experiment, using an intermediate modified scheme, is conducted to aid the understanding of the results. In this experiment, supersaturation is permitted by simply increasing the ice saturation mixing ratio used in the cloud scheme to the critical value given by Koop et al. (2000), in other words, the saturation clipping limit is replaced by $RH_{crit}q_s$ in the ice phase, with cloud formation commencing when the grid-mean humidity exceeds $K.RH_{crit}q_s$. Ice crystal growth in this case can only reduce the humidity back to this higher critical value.

The model integrations are validated in terms of normalized probability density functions (PDFs) of relative humidity (with respect to ice), which are compared to the MOZAIC climatological PDFs given by Gierens et al. (1999). Results are shown at the 250 hPa level for latitudes less than 60^o, using the last month of the climate integrations, with data archived once daily. All PDFs are normalised such that $PDF(RH = 100\%) = 1$. The high latitudes are excluded to avoid confusing tropospheric and stratospheric air masses in the statistics.

Fig. 4 compares the new scheme to the default model. The default model behaves as expected, with a sharp mode around $RH = 1$ due to the fact that this limit can not be exceeded in cloudy air masses. There is a slight overshoot with RH attaining values up to almost 10% supersaturation. This is a purely numerical effect, and among other causes, is the result of the clipping to saturation in the model not being performed at exact "end of time-step" temperature and humidity profiles with semi-Lagrangian dynamics in use. The third experiment with the increased nucleation threshold responds as expected, with the PDF shifted to the right and a broader

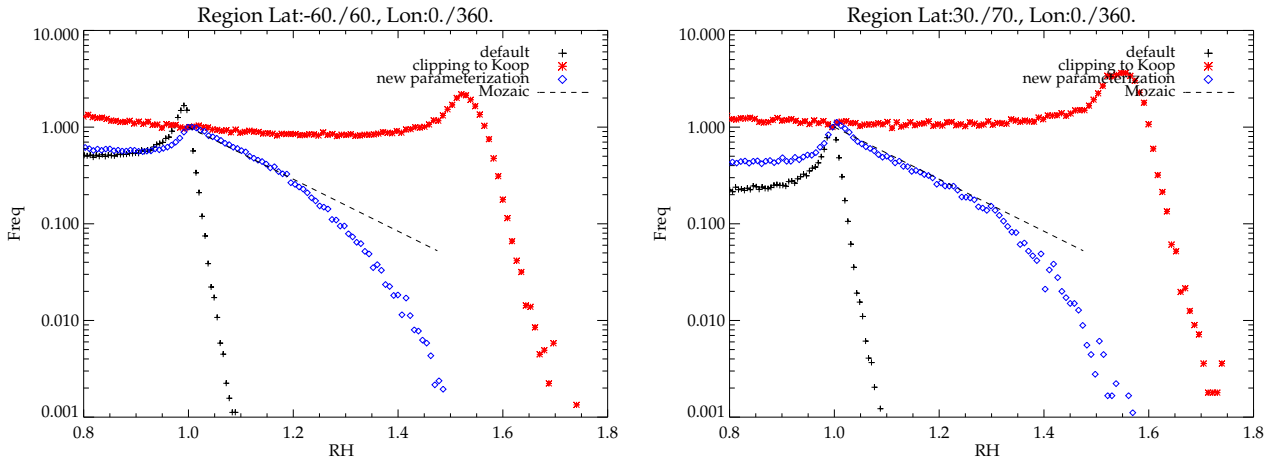

Figure 4: Normalised PDF of RH at the 250 hPa level for (left) latitudes less than 60 degrees and (right) northern hemisphere only. Observations and models are identified in the legend.

mode existing around the 50 to 60% supersaturation appropriate for this pressure level. The mode is broader than the control due to the additional dependence of RH_{crit} on temperature.

The new parametrisation produces a PDF of RH that lies somewhere between these two extremes. After the smaller 100% mode, the data follows the best-fit line to the observations made in the MOZAIC campaign. However, at a supersaturation of around 20% the PDF becomes steeper than the observations, that is, relative to the frequency of occurrence at 100%RH, fewer grid-points attain high values of relative humidity. A comparison for the Northern Hemisphere mid-latitude reveals a similar picture, with the MOZAIC data followed closely to the scale break occurring at around 130%RH.

The scale break did not occur in the scheme of Lohmann and Kärcher (2002) which reproduced the aircraft data well out to the observed limit of around 160%RH. This disparity between the two models can be explained by the their treatment of sub grid-scale variability. The MOZAIC data used by Gierens et al. (1999) was averaged over 60 seconds, equivalent to a horizontal length scale of 15km; much smaller than the grid-size of the GCM. However, if the GCM were to neglect subgrid variability, then it would be expected to reproduce the observations. It is recalled that the *grid-mean* value of humidity is used to initiate ice nucleation in the Lohmann and Kärcher (2002) scheme, which essentially means that the subgrid variability is neglected. The IFS model makes a very simple assumption that the environmental humidity (which can be larger than the in-cloud value) can already initiate ice nucleation when it reaches 80% of the critical threshold, due to subgrid fluctuations. It is clear that 80% of the average threshold of very roughly 160% supersaturation is around 130%, which is approximately the scale-break threshold. Analysis of the 150 and 200 hPa levels produced similar results (not shown).

4.3 Contrail predictions

Since the new parametrization aims to improve the representation of supersaturation in the humidity field at cold temperatures, it is likely and desirable that more accurate predictions of occurrence of persistent aircraft condensation trails (contrails) should result. Contrails are recognised to influence the Earth's radiative budget by having a warming effect (IPCC, 1999), which, while currently minor, may become more important with future projections of increasing air traffic. Moreover, persistent contrails may spread out and form cirrus clouds that are difficult to distinguish from naturally formed clouds, and thus have a more important effect than currently

estimated. In order to study these issues it is extremely important to have a model that does have skill to predict contrail formation and their persistence.

In order for contrails to form and persist for more than a few minutes certain atmospheric conditions have to be fulfilled (Schumann, 1996; Jensen et al., 1998). The atmosphere at the altitude of the aircraft has to be supersaturated with respect to ice and the ambient air temperature has to be sufficiently low. The exact maximum temperature that allows contrail formation depends on engine parameters, pressure and ambient humidity. For our purpose here, however, it can be reasonably and simply assumed that T must not exceed 233 K, the approximate threshold for the onset of homogeneous nucleation of aqueous solution drops (Pruppacher and Klett, 1997).

Applying these two simple criteria using the default model and the new parametrisation a hit/miss prediction for the existence of persistent contrails is made. The predictions derive from six months worth of short term forecasts, which are compared to a long-term dataset of local visual contrail observations, taken over Reading in Southern UK. Weather conditions permitting, these observations have been taken since July 2004 on a quasi-regular basis, (usually four times a day), using a three category classification according to the presence of permanent, non-permanent or no contrails. A full description of the contrail observation set will be given in a separate article which addresses the predictive skill of radiosonde relative humidity soundings, hence only a brief description is given here. Reading is particularly well suited to establish such a contrail database due to its geographical location at the entrance of the North-Atlantic flight corridor. In this study we use observations between August 2004 and January 2005, inclusive.

For the purpose of model validation the three categories were condensed into two states of 'yes'-events where permanent contrails were observed, and 'no'-events (non-permanent or no contrail observed). A statistical analysis has been performed by comparing both categories to the model predictions for contrail favourable or non-favourable atmospheric conditions. For this, a simple relative humidity threshold is used of $\langle RH_{\mathrm{ice}} \rangle > 99\%$ and $\langle T \rangle < 233$ K, where $\langle RH_{\mathrm{ice}} \rangle$ and $\langle T \rangle$ are obtained from a forecast initialised at 12 UTZ at a forecast range between 20 to 30 hours to coincide with the exact observation time, for the grid box containing Reading. The threshold of 99% for $\langle RH_{\mathrm{ice}} \rangle$ was applied since the default model clips $\langle RH_{\mathrm{ice}} \rangle$ at 100%, with the 1% difference allowing for inaccuracies in numerics and archiving.

When making the comparison, it is important to recall that the observation is made for the visible all-sky hemisphere, which will not correspond to the same region as a model T511 gridbox with a resolution of approximately 40 km. Moreover, the observation is classified as a 'hit' if a permanent contrail is visible anywhere in the sky. Horizontal (and indeed vertical) variability of humidity means that permanent contrails and ice subsaturated conditions may coexist within the observational domain, implying that a lower RH threshold may lead to increased contrail predictive skill. These issues will be explored further in a separate paper analysing radiosonde predictions. Here only the single threshold is used for reasons of brevity, which is justifiable since two model versions are compared using this identical benchmark. While greater or lesser skill may be achieved with other thresholds, the sign of the sensitivity of the prediction skill to parametrization methodology is robust.

The result of each set of comparisons can be represented in a 2×2 contingency table, yielding the number of correct hits (a), false alarms (b), number of misses (c) and lastly the number of correct rejections (d). A possible method to compute the statistical significance of these results is the 'odds ratio', proposed by Stephenson (2000) for meteorological applications. The odds ratio, R, is defined as

$$R = \frac{a \cdot d}{b \cdot c}.$$

This metric is equal to unity if there is no correlation between prediction and observation, larger than 1 for the case of a positive correlation and smaller than 1 for a negative correlation. The natural logarithm of R is

Default model:			new cloud scheme		
	observed			observed	
	yes	no		yes	no
predicted			predicted		
yes	31	38	yes	41	28
no	12	71	no	16	67

Table 2: 2×2 *contingency tables for comparisons of visual contrail observations with predictions using the default model (left) or the new parametrisation (right)*

asymptotically Gaussian distributed, with a standard deviation of

$$\sigma = \sqrt{\frac{1}{a} + \frac{1}{b} + \frac{1}{c} + \frac{1}{d}}.$$

The two contingency tables for the default model and the new parametrisation are given in table 2. It can be seen that the new parametrisation predicts persistent contrails more often than the default model: the hit-rates $(a/(a+c))$ are 0.59 for the new parametrisation and 0.45 for the default model, but also the false-alarm rate $(b/(b+d))$ increases from 0.14 to 0.19. The odds ratio takes into account all this information and it increases from 4.8 to 6.1 by going from the default to the new parametrisation. The significance of these result can be tested by comparing it to the null hypotheses that the forecast and the observations are independent of each other with a log(odds) of zero. While the log(odds) of the forecast using the default model is 3.99 standard deviations away from zero, it is 4.89 for the new parametrisation. Hence, clearly an improvement in significance has been achieved.

4.4 Analysis experiments

In summary, the main impact of the new parametrization in the model climate is to allow supersaturation with respect to ice, oft documented by in-situ aircraft data and satellite retrievals, and also that the high level cloud cover is reduced in the tropics. The code was subsequently tested in data assimilation mode for a period of many months [4]. Overall the new cloud scheme is scores neutral (not shown).

One feature of the assimilation worth highlighting is the impact in the analysis on the relative humidity. As expected from the analysis of the model climate in Fig. 3, the departure statistics indicate a significant impact of the new ice scheme for this variable, with a significant moistening of the analysis in the upper troposphere. Figures 5, 6 and 7 show that, while the upper-tropospheric bias appears to be improved relative to radiosondes in the NH, the reverse appears to be true in the tropics and SH where the default model was already apparently suffering from a moist bias relative to the sondes. Moreover, the standard deviation of the departures has also increased.

While these statistics appear to show that the new scheme has worsened existing upper-tropospheric moist biases, it should be highlighted that the radiosonde humidity profiles are not subjected to any bias correction. It is firmly established that in the upper-troposphere, commonly used radiosonde devices suffer from significant

[4] the code was combined with other cloud scheme changes designed to eradicate vertical resolution sensitivities in the cloud scheme. These include an implicit solver for the cloud scheme numerics to allow ice to sediment through many levels in a single timestep, and the introduction of an explicit snow autoconversion generation term for compatibility with the new ice assumptions. These changes are documented in technical memorandum R60.3/AT/0599, "Revised cloud scheme to reduce sensitivity to vertical resolution"

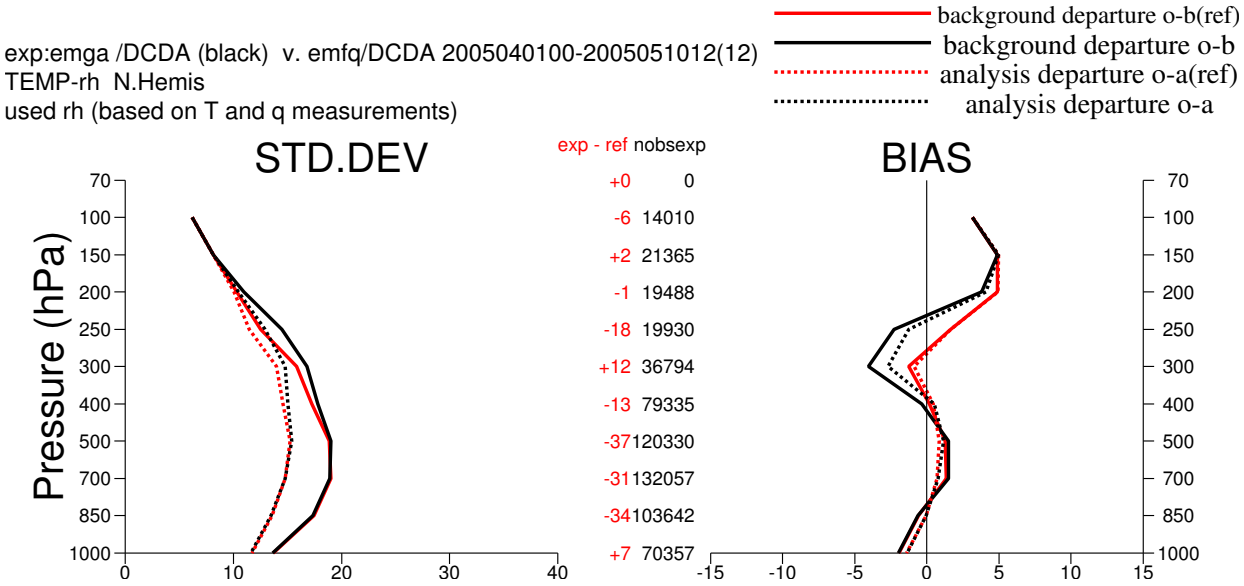

Figure 5: Northern Hemisphere (latitude > 20N) mean Bias (right) and standard deviation (left) of RH departures compared to the used radiosonde measurements (marked 'o' for 'observations') in the background (i.e. the first guess) and analysis of the standard model (red lines) and model incorporating the new supersaturation scheme (black lines)

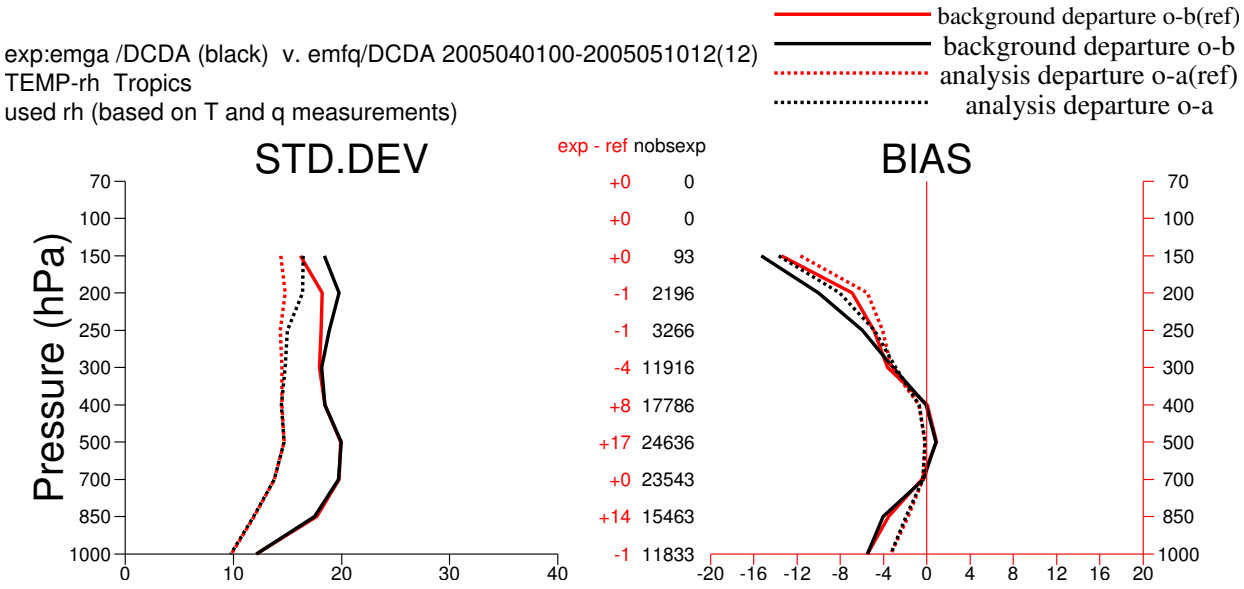

Figure 6: As Fig. 5, but for the tropics (20S<latitude<20N)

dry biases (e.g. Soden and Lanzante, 1996; Wang et al., 2002; John and Buehler, 2005). The results of an in-depth humidity study by Soden et al. (2004) highlighted significant dry biases of up to 40% in radiosonde upper troposphere humidity measurements. Soden et al. (2004) moreover pointed out that established bias correction techniques such as derived by Wang et al. (2002), which can add up to 15% *RH* in the upper troposphere, were nevertheless not effective at correcting all of the bias.

It is thus likely that the new cloud scheme is actually improving the upper tropospheric humidity fields, while the dry-biased sonde data counteracts this affect, as seen in Fig. 7 where the analysis is drier than the first guess due to their influence. In support of this hypothesis are the comparisons of ECMWF analysed humidity fields

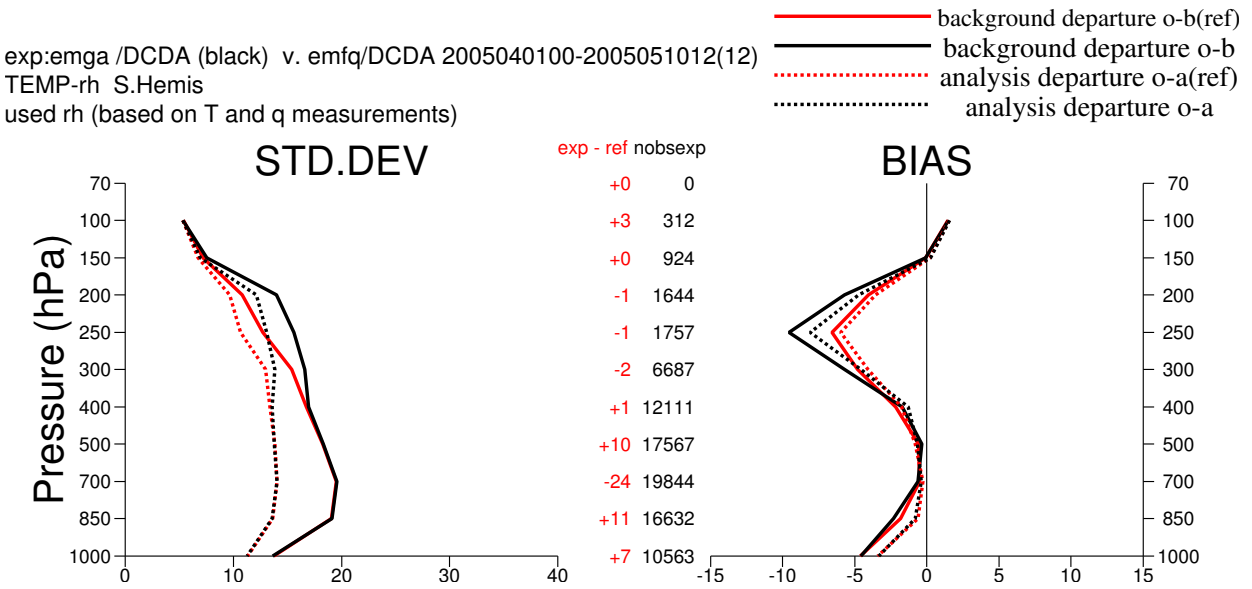

Figure 7: As Fig. 5, but for the southern hemisphere (20S)

to two different in-situ aircraft datasets by Ovarlez et al. (2000) and Nawrath (2002). Both studies claim that the ECMWF analysis is biased dry in the upper troposphere by at minimum of 10%, indicating that the new scheme indeed improves the humidity fields significantly.

5 Conclusions

First results are presented from a new and simple parametrisation that attempts to represent ice supersaturation and the homogeneous ice nucleation process. The model contrasts to existing schemes in that it does not attempt to explicitly model the nucleation and deposition process. Rather it assumes that the process is fast compared to a GCM time-step so that one can diagnostically perform an instantaneous adjustment to saturated conditions inside the cloud once nucleation initiates. It is argued that without an additionally prognostic equation to provide the ability to separately map the evolution of the humidity within the cloud and in the environment, schemes that attempt to explicitly model the deposition process are forced to make a diagnostic assumption to distribute the grid mean humidity between the cloud and clear-sky portions of the grid cell at each time-step. The assumptions used in existing schemes were reviewed, and were seen to differ greatly, indicating their often ad-hoc nature. Their derivation often neglects the impact of microphysics which can imply a significant and totally artificial horizontal flux of water vapour between the clear-sky and cloudy portions of the grid cell between time-steps, which can dominate the microphysical processes. It is therefore argued that within the constraints of current schemes that do not implement a separate prognostic equation for in-cloud humidity, that the scheme outlined here provides a simple alternative approach, albeit at the expense of not allowing ice crystals to exist in subsaturated conditions.

Although extremely crude and simple, the new scheme agrees well with aircraft observations at the lower range of supersaturations (up to relative humidities of 120 to 130%), while it under-predicts the occurrence of higher *RH* values, as indeed it should since the observations are collected at a smaller horizontal spatial scale. The threshold at which the model and aircraft observations begin to diverge is consistent with the simple assumptions the model makes concerning the sub grid fluctuations of humidity and temperature.

The main effect on the model climate is to reduce the high cloud cover, most prominently in the Tropics. The humidity field is also influenced, with the upper-troposphere moistened globally with the new scheme as expected. While this appears to conflict with evidence from radiosonde data, which document an existing moist bias in the operational model, it is pointed out that the radiosonde data itself is not bias-corrected in the ECMWF analysis system, while many investigations have established a significant dry bias in sonde measurements. The moistening of the upper troposphere by the new scheme is likely to represent an improvement, since the model is apparently biased dry compared to in-situ aircraft measurements. In further support it is shown that the new scheme also significantly improves the prediction of permanent contrail occurrence over southern England. It is therefore a recommendation of this work that ECMWF attempts to monitor and quantify the magnitude of this upper-tropospheric, lower-stratospheric dry bias, and if possible take subsequent steps to apply a suitable bias correction in the data assimilation system.

Acknowledgements

The first author would express his appreciation to both Ulrike Lohmann (ETH, Zurich) and Damian Wilson (Met Office, UK) for their insightful comments and many vigorous discussions that have focused on the merits of the various approaches to cloud parametrization, and which took place during various workshops and meetings, in addition to visits to their respective host institutes. Further discussions with Bernd Kärcher, Keith Shine and Peter Spichtinger were also much appreciated. This work contributes to the DLR (German Aerospace Centre) project Particles and Cirrus Clouds (PAZI-2). The third author is supported by the UK Department of Trade and Industry and Airbus.

References

Bony, S. and K. A. Emanuel, 2001: A parameterization of the cloudiness associated with cumulus convection; Evaluation using TOGA COARE data, *J. Atmos. Sci*, **58**, 3158–3183.

Gierens, K., 2003: On the transition between heterogeneous and homogeneous freezing, *Atmos. Chem. Phys.*, **3**, 437–446.

Gierens, K., R. Kohlhepp, P. Spichtinger, and M. Schrödter-Homscheidt, 2004: Ice supersaturation as seen from TOVS, *Atmos. Chem. Phys.*, **4**, 539–547.

Gierens, K., U. Schumann, M. Helten, H. Smit, and A. Marenco, 1999: A distribution law for relative humidity in the upper troposphere and lower stratosphere derived from three years of MOZAIC measurements, *Ann. Geophysicae*, **17**, 1218–1226.

Gierens, K., U. Schumann, M. Helten, H. Smit, and P. H. Wang, 2000: Ice-supersaturated regions and subvisible cirrus in the northern midlatitude upper troposphere, *J. Geophys. Res.*, **105**, 22743–22753.

Heymsfield, A. J., L. M. Miloshevich, C. Twohy, G. Sachse, and S. Oltmans, 1998: Upper-tropospheric relative humidity observations and implications for cirrus ice nucleation, *Geophys. Res. lett.*, **25**, 1343–1346.

IPCC, 1999: Aviation and the Global Atmosphere - A Special Report of IPCC Working Groups I and III, eds. Penner J. E. et al., Technical report, IPCC.

Jakob, C., 2000: *The representation of cloud cover in atmospheric general circulation models*, Ph.D. thesis, University of Munich, Germany, available from ECMWF, Shinfield Park, Reading RG2 9AX, UK.

Jensen, E. J., O. B. Toon, S. Kinne, G. W. Sachse, B. E. Anderson, K. R. Chan, C. H. Twohy, B. Gandrud, A. J. Heymsfield, and R. C. Miake-Lye, 1998: Environmental conditions required for contrail formation and persistence, *J. Geophys. Res.*, **103**, 3929–3936.

John, V. O. and S. A. Buehler, 2005: Comparison of microwave satellite humidity data and radiosonde profiles: A survey of European stations, *Atmos. Chem. Phys.*, **5**, 1843–1853.

Jung, T., A. M. Tompkins, and M. J. Rodwell, 2005: Some aspects of systematic error in the ECMWF model, *Atmos. Sci. Lett.*, **6**, 133–139.

Kärcher, B. and U. Lohmann, 2002: A parameterization of cirrus cloud formation: Homogeneous freezing of supercooled aerosols, *J. Geophys. Res.*, **107**, DOI: 10.1029/2001JD000470.

Khvorostyanov, V. and K. Sassen, 1998: Cirrus cloud simulation using explicit microphysics and radiation. Part II: Microphysics, vapor and ice mass budgets, and optical and radiative properties, *J. Atmos. Sci.*, **55**, 1822–1845.

Koop, T., B. P. Luo, A. Tsias, and T. Peter, 2000: Water activity as the determinant for homogeneous ice nucleation in aqueous solutions, *Nature*, **406**, 611–614.

Li, J.-L., D. E. Waliser, J. H. Jiang, D. L. Wu, W. Read, J. W. Waters, A. M. Tompkins, L. J. Donner, J. D. Chern, W. K. Tao, R. Atlas, Y. Gu, K. N. Liou, A. Del Genio, M. Khairoutdinov, and A. Gettelman, 2005: Comparisons of EOS MLS cloud ice measurements with ECMWF analyses and GCM simulations: Initial results, *Geophys. Res. Lett.*, **32**, L18710, doi:10.1029/2005GL023788.

Lin, R.-F., D. Starr, P. J. DeMott, R. Cotton, K. Sassen, E. Jensen, B. Kärcher, and X. Liu, 2002: Cirrus Parcel Model Comparison Project. Phase 1: The Critical Components to Simulate Cirrus Initiation Explicitly, *J. Atmos. Sci.*, **59**, 2305–2329.

Lin, Y. L., R. D. Farley, and H. D. Orville, 1983: Bulk parameterization of the snow field in a cloud model, *J. Climate Appl. Meteor.*, **22**, 1065–1092.

Lohmann, U. and B. Kärcher, 2002: First interactive simulations of cirrus cloud formed by homogeneous freezing in the ECHAM general circulation model, *jgr*, **107**, 10.1029/2001JD000767.

Nawrath, S., 2002: *Water vapor in the tropical upper troposphere: On the influence of deep convection*, Ph.D. thesis, University of Cologne, pp. 120.

Ovarlez, J. and P. van Velthoven, 1997: Comparison of water vapor measurements with data retrieved from ecmwf analyses during the polinat experiment, *J. Appl. Meteor.*, **36**, 1329–1335.

Ovarlez, J., P. van Velthoven, G. Sachse, S. Vay, H. Schlager, and H. Ovarlez, 2000: Comparison of water vapor measurements from POLINAT 2 with ECMWF analyses in high-humidity conditions, *J. Geophys. Res.*, **105**, 3737–3744.

Pruppacher, H. R. and J. D. Klett, 1997: *The Microphysics of Clouds and Precipitation*, Kluwer Academic Publishers, pp. 954.

Rädel, G., C. J. Stubenrauch, R. Holz, and D. L. Mitchell, 2003: Retrieval of effective ice crystal size in the infrared: Sensitivity study and global measurements from TIROS-N Operational Vertical Sounder, *J. Geophy. Res.*, **108**, 10.1029/2002JD002801.

Ren, C. and A. R. Mackenzie, 2005: Cirrus parametrization and the role of ice nuclei, *Q. J. R. Meteorol. Soc.*, **131**, 1585–1605.

Rossow, W. B. and R. A. Schiffer, 1991: ISCCP cloud data products, *Bull. Amer. Meteor. Soc.*, **72**, 2–20.

Rossow, W. B. and R. A. Schiffer, 1999: Advances in understanding clouds from ISCCP, *Bull. Amer. Meteor. Soc.*, **80**, 2261–2287.

Schumann, U., 1996: On conditions for contrail formationfrom aircraft exhausts, *Meteorol. Zeitschrift*, **5**, 4–25.

Simmons, A. J., A. Untch, C. Jakob, P. Kallberg, and P. Undén, 1999: Stratospheric water vapour and tropical tropopause temperatures in ECMWF analyses and multi-year simulations, *Q. J. R. Meteorol. Soc.*, **125**, 353–386.

Smith, R. N. B., 1990: A scheme for predicting layer clouds and their water-content in a general-circulation model, *Q. J. R. Meteorol. Soc.*, **116**, 435–460.

Soden, B. J. and J. R. Lanzante, 1996: An assessment of Satellite and radiosonde climatologies of upper-tropospheric water vapor, *J. Climate*, **9**, 1235–1250.

Soden, B. J., D. D. Turner, B. M. Lesht, and L. M. Miloshevich, 2004: An analysis of satellite, radiosonde, and lidar observations of upper tropospheric water vapor from the Atmospheric Radiation Measurement Program, *J. Geophys. Res.*, **109**, D04105, doi:10.1029/2003JD003828.

Spice, A., D. W. Johnson, P. R. A. Brown, A. G. Darlison, and C. P. R. Saunders, 1999: Primary ice nucleation in orographic cirrus clouds: A numerical simulation of the microphysics, *Q. J. R. Meteorol. Soc.*, **125**, 1637–1667.

Spichtinger, P., K. Gierens, and W. Read, 2003: The global distribution of ice-supersaturated regions as seen by the Microwave Limb Sounder, *Q. J. R. Meteorol. Soc.*, **129**, 3391–3410.

Stephenson, D. B., 2000: Use of the 'Odds Ratio' for Diagnosing Forecast Skill, *Wea. and Forecasting*, **15**, 221–232.

Tiedtke, M., 1993: Representation of clouds in large-scale models, *Mon. Wea. Rev.*, **121**, 3040–3061.

Tompkins, A. M., 2002: A prognostic parameterization for the subgrid-scale variability of water vapor and clouds in large-scale models and its use to diagnose cloud cover, *J. Atmos. Sci.*, **59**, 1917–1942.

Tompkins, A. M., P. Bechtold, A. Beljaars, A. Benedetti, S. Cheinet, M. Janisková, M. Köhler, P. Lopez, and J.-J. Morcrette, 2004: Moist physical processes in the IFS: Progress and Plans, *ECMWF Technical Memorandum*, **452**, available at http://www.ecmwf.int/publications/.

Wang, J. H., H. L. Cole, D. J. Carlson, E. R. Miller, K. Beierle, A. Paukkunen, and T. K. Laine, 2002: Corrections of humidity measurement errors from the Vaisala RS80 radiosonde - Application to TOGA COARE data, *J. Atmos. Ocean. Tech.*, **19**, 981–1002.

Wilson, D. and R. Forbes, 2004: The large-scale precipitation parametrization scheme, Technical report, Met Office, Fitzroy Rd, Exeter, EX1 3PB, UK, Unified model documentation paper 26.